[3] R. M. Broudy, "Study to improve the low frequency noise characteristics of (Hg, Cd)Te detectors," Final Tech. Rep. (Apr. 1971–Aug. 1973), NASA Contract No. NAS1-10682.
[4] T. J. Tredwell, "Advances in 2 to 5-μm (Hg, Cd)Te photodiodes," in *1976 Int. Electron Devices Meeting Proc.* (Washington, DC, Dec. 1976).
[5] T. J. Tredwell, *Opt. Eng.*, vol. 16, p. 237, 1977.
[6] A. Sood and T. Tredwell, in *1978 Int. Electron Devices Meeting Proc.*, (Washington, DC, Dec. 1978).
[7] R. Broudy, M. Gurnee, S. Iwasa, T. Tredwell, and J. White, "IR/CCD hybrid focal planes," *S.P.I.E. Proc.*, vol. 132, "Utilization of infrared detectors," 1978.
[8] See, for example, A. van der Ziel and E. Chenette, in *Advances in Electronics and Electron Devices*, vol. 46, L. Marton, Ed. New York: Academic Press, 1978.
[9] A. L. McWhorter, "1/f noise and germanium surface properties," in *Semiconductor Surface Physics* (U. Penn., 1957) p. 207.
[10] V. E. Noble and J. E. Thomas, *J. Appl. Phys.*, vol. 32, p. 1709, 1961.
[11] T. B. Watkins, *Proc. Phys. Soc.*, vol. 73, p. 59, 1954.
[12] M. M. Atalla, E. Tannenbaum, and E. J. Scheibner, *Bell Syst. Tech. J.*, vol. 38, p. 749, 1959.
[13] C. T. Sah and F. H. Hielscher, *Phys. Rev. Lett.*, vol. 17, p. 956, 1966.
[14] L. M. Terman, *J. Solid State Electron.*, vol. 5, p. 285, 1962.
[15] E. H. Nicollian and H. Melchior, *Bell Syst. Tech. J.*, vol. 46, p. 1055, 1967; and vol. 46, p. 2019, 1967.
[16] H. Prier, *Appl. Phys. Lett.*, vol. 10, p. 3611, 1967.
[17] S. Christensson, I. Lundstrom, and C. Svensson, *Solid-State Electron.*, vol. 11, p. 797, 1968; and vol. 11, p. 813, 1968.
[18] S. T. Hsu, *Solid-State Electron.*, vol. 13, p. 1451, 1970.
[19] —, *Appl. Phys. Lett.*, vol. 12, p. 287, 1968.
[20] —, *Solid-State Electron.*, vol. 13, p. 843, 1970.
[21] F. R. Pierret, *Solid-State Electron.*, vol. 17, p. 257, 1974.

Effect of Trap Tunneling on the Performance of Long-Wavelength $Hg_{1-x}Cd_xTe$ Photodiodes

JACOB Y. WONG

Abstract—**The effect of trap tunneling on the detector performance of long cutoff wavelength (λ_{co}) $Hg_{1-x}Cd_xTe$ photodiodes was investigated with the use of a parametric model. The development of this model follows closely the formulation by Sah for treating the case of excess currents in gold-doped narrow silicon junctions. The trap tunneling limited R_0A's for long-wavelength $Hg_{1-x}Cd_xTe$ photodiodes with different p- and n-side doping concentrations and at different temperatures were calculated using this model as a function of p-side trap density, trap location, and junction impurity concentration gradient. The calculated results are in agreement with those measured from actual photodiodes. In particular, the somewhat unexpected temperature dependence of the measured R_0A product at low-temperatures can be satisfactorily accounted for. The present tunneling model also adequately explains the observed soft reverse breakdown characteristics for these devices and their behavior as a function of temperature.**

I. Introduction

THE RECENT advent of hybrid assemblies of conventional silicon CCD's and infrared detectors has generated interest in their application to strategic-surveillance sensor programs in the form of imaging infrared focal plane arrays (FPA's) [1]-[4]. Aside from the rapid advances in the areas of CCD readout and signal-processing techniques to infrared arrays (both hybrid [5]-[8] and monolithic [9]-[11]), the basic infrared photodetector technology itself is making impressive gains [12]-[14]. Mercury cadmium telluride ($Hg_{1-x}Cd_xTe$) has emerged over the past decade as the single most promising infrared quantum detector material, primarily because it is an intrinsic semiconductor and also because its chemically adjustable bandgap (hence λ_{co}) spans the important 2- to 30-μm spectral region.

Present state-of-the-art long-wavelength infrared (LWIR) PV $Hg_{1-x}Cd_xTe$ detectors have R_0A product values which indicate diffusion limited operation at 77 K [13]. (At low backgrounds or at high operating temperatures, $D^*(\lambda)$ is directly proportional to the square root of R_0A where R_0 is the zero-bias dynamic resistance of the photodiode and A is the active area of the detector.) One of the current impeti in this area of detector research has been to extend the photodiode spectral response to longer wavelengths by fabricating these devices out of narrower bandgap $Hg_{1-x}Cd_xTe$ materials, and also by operating them at lower temperatures. Although the performance for these LWIR PV $Hg_{1-x}Cd_xTe$ detectors is expected to be limited by the generation-recombination (g-r) current noise originating in the space-charge region, the achievable R_0A products for photodiodes with $\lambda_{co} > 12$ μm and operating at temperatures below 77 K are generally well below those expected from g-r noise limited operation. While

Manuscript received May 21, 1979; revised August 10, 1979.
The author is with the Santa Barbara Research Center, Goleta, CA.

0018-9383/80/0100-0048$00.75

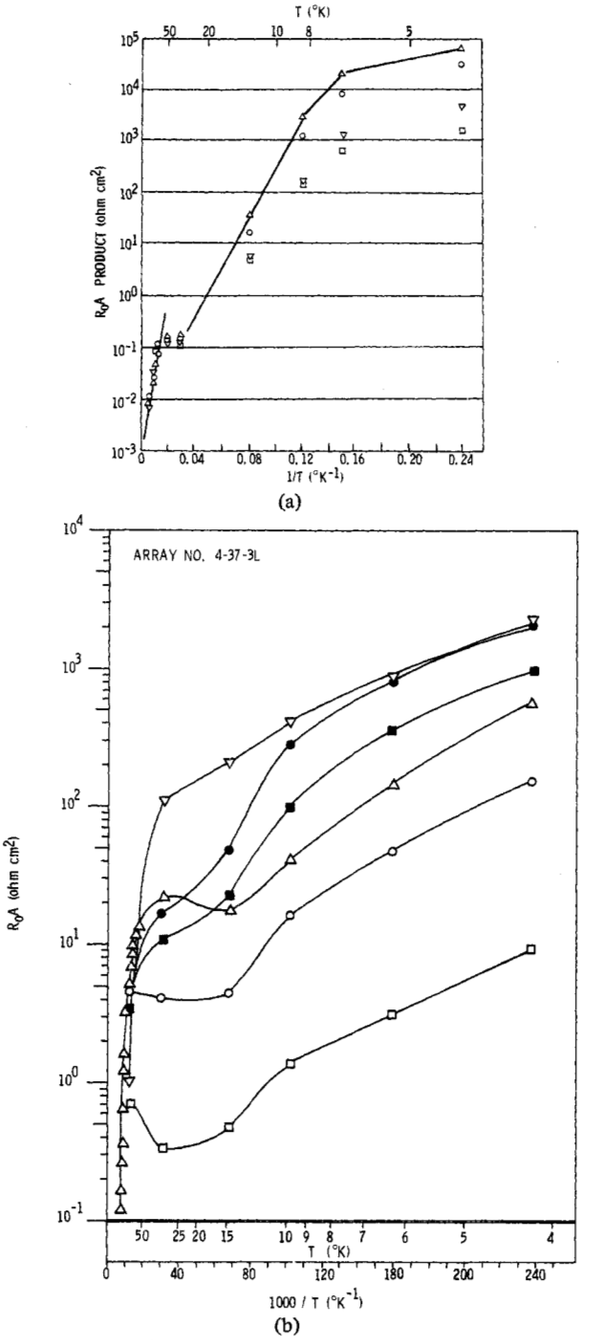

Fig. 1. (a) Measured R_0A versus temperature data for four randomly selected HgCdTe PV detectors with λ_{co} (77 K) ~ 12.3 μm [17]. (b) Measured R_0A versus temperature data for six randomly selected HgCdTe PV detectors with λ_{co} (77 K) ~ 10.5 μm [17].

the overall disappointing performance of these long-wavelength photodiodes can, in general terms, be attributed to surface leakage of as yet undetermined origins, there are two characteristics exhibited by nearly all of these devices that cannot presently be explained satisfactorily. First, nearly all of these devices show a plateau in R_0A value from 70 K down to about 40 K and then a gradual increase toward lower temperatures as seen in Fig. 1. Fig. 1(a) shows the R_0A product versus temperature curves for four randomly selected $Hg_{1-x}Cd_xTe$ photodiodes from a boron-implanted n-on-p detector array with a $\lambda_{co} \approx 12.3\ \mu$m at 77 K. These are planar diodes fabricated out of randomly oriented bulk $Hg_{1-x}Cd_xTe$ crystals having an active area of 5×10^{-4} cm^2. The concentration for the base acceptors and the implanted donors is 5×10^{15} cm^{-3} and $5\text{-}10 \times 10^{15}$ cm^{-3}, respectively. Fig. 1(b) shows more of the same data for six stoichiometric diodes with a $\lambda_{co} \approx 10.5$ μm at 77 K. These diodes have n- and p-side dopings ranging from 5×10^{14} to 1×10^{15} cm^{-3}. Notice the characteristic minima in R_0A value between 70 and 15 K exhibited by nearly all the devices shown in Fig. 1. Notice also the widely scattered R_0A values for different devices having R_0A minima at different temperatures. This temperature dependence of the R_0A product cannot be explained by a g-r current mechanism which is expected to be operative for these devices at these temperatures. Nor can any presently known surface leakage mechanism explain such temperature behavior.

Second, most of these long-wavelength photodiodes possess soft reverse-breakdown characteristics. Moreover, the reverse saturation current for some of these devices goes through a maximum somewhere between 30 and 60 K and then starts to decrease toward lower temperatures [15]. Again, this rather peculiar temperature behavior of the reverse characteristics cannot be adequately accounted for by any known surface leakage mechanisms. The independent operation of one or more as yet unidentified physical processes (surface or bulk) might be responsible for the observed temperature data of these photodiodes.

The significance of tunneling contribution to noise in PV detectors of small-bandgap materials such as $InAs_{1-x}Sb_x$ ($0 < x \leq 0.2$) had been pointed out earlier [16]. It was shown that for heavily doped photodiodes detectivity performance can be severely limited by interband tunneling. The same situation had been shown to hold true for long-wavelength $Hg_{1-x}Cd_xTe$ photodiodes with heavily doped p and n sides ($p \geq 10^{18}$ cm^{-3} and $n \geq 10^{17}$ cm^{-3}) [17]. For doping levels comparable to those used in the fabrication of presently discussed long-wavelength photodiodes (10^{15} cm$^{-3} < p, n < 10^{16}$ cm^{-3}) calculations showed that interband tunneling is not an important mechanism that limits the R_0A product [16], [17]. Moreover, had interband tunneling been an important current process it still would not explain the temperature dependence of the R_0A product, the soft reverse-breakdown characteristics and the peculiar behavior of the reverse saturation current as a function of temperature for these devices.

In the present paper, the tunneling of electrons from acceptor traps on the p side to the conduction band on the n-side and the role it plays in limiting the achievable R_0A product for long-wavelength $Hg_{1-x}Cd_xTe$ photodiodes are investigated in detail. The development of the parametric model used in the calculation of trap tunneling limited R_0A for these devices follows closely that formulated by Sah in treating the case of excess currents in gold-doped narrow silicon junctions [18]. The trap tunneling mechanism is presented in Section II. A parametric trap tunneling model is developed quantitatively in Section III. Section IV is devoted to the calculation of trap tunneling limited R_0A for long-wavelength $Hg_{1-x}Cd_xTe$ photodiodes with different p- and n-side dopings and at differ-

ent temperatures as a function of p-side trap density, trap location, and the junction impurity concentration gradient. The results of this calculation are discussed in Section V together with suggestions for further verification and extension of the present model.

II. Trap Tunneling Mechanism

The trap tunneling process considered in this paper involves electrons tunneling directly from the occupied trap states on the p side to the empty band states on the n side of the p-n junction. The likelihood of occurrence for such a quantum-mechanical process depends upon a number of factors. First, the trap states (initial states) on the p side of the junction must be sufficiently populated so that a relatively large number of electrons can participate. Implicitly, the rate of tunneling from trap states must be smaller than the rate of filling the traps. For acceptor-type traps on the p side, the occupancy depends upon the location of the quasi-Fermi level in conjunction with a Hall-Shockley-Read type process. Second, the probability for direct traps-to-band states tunneling across the forbidden gap must be reasonably large. This tunneling probability depends not only upon the height and width of the potential barrier that the electrons must surmount but also upon the effective mass of these electrons in the semiconductor material. The values for the height and width of the potential barrier are directly related to the characteristics of the p-n junction, including the doping concentrations on the p and n side and the junction impurity profile. The effective mass of the tunneling electrons is a material parameter, which for $Hg_{1-x}Cd_xTe$ is both a function of temperature and the chemical composition x. Third, the conservation of total energy and total momentum for the tunneling electrons must be rigorously enforced. Fourth, there must exist sufficient empty band states (final states) on the n side of the junction to accommodate the tunneling electrons for completing the process.

The role played by the device junction temperature in the overall trap tunneling process is an important one since the factors mentioned above that govern the probability of this process are all strongly temperature dependent. The biasing condition for the photodiode is also important in that it determines the locations of the quasi-Fermi levels (Imrefs) on both sides of the junction during the device operation. Thus the number of electrons participating in the trap tunneling, the nature of the barrier potential, the electron effective mass, and the density of empty final states are all directly related to the device junction temperature and its biasing condition.

In the following paragraphs we shall investigate in more detail all the factors mentioned above when applied to long-wavelength $Hg_{1-x}Cd_xTe$ photodiodes as a means of determining the likelihood of trap tunneling taking place in these devices.

The occurrence of acceptor trap states in p-type $Hg_{1-x}Cd_xTe$ material, in addition to the usual crystalline defects, such as dislocations, interstitially or substitutionally located impurity atoms, vacancies, etc., can take on various and more abundant forms dependent upon the nature of the dopants. For both Au-diffused p-type material, where the acceptor concentration is controlled by the solid solubility of Au as a function of diffusion temperature, and p-type material whose conductivity is determined by the equilibrium concentration of Hg vacancies at the annealed temperature, each acceptor level provides a potential trap site for the presently considered tunneling process. The exact location of these singly ionized Au acceptor levels (Au^+) and native acceptor defects, in this case Hg vacancies, is not known at present. However, experimental study of the increase in series resistance for junction devices as a function of decreasing temperature attributable to the freezeout of holes indicates a range from a few to slightly less than 10 meV above the valence band edge [13]. For p-type material in which the doping is due to residual foreign-atom acceptor impurities, the potential trap sites include not only the active acceptor levels lying close to the top of the valence band but also other Shockley-Read type recombination centers that are distributed in energy throughout the bandgap. The occupancy of these latter acceptor centers is governed by the Hall-Shockley-Read recombination statistics and is, therefore, a function of both the temperature and their exact locations above the top of the valence band. For long-wavelength $Hg_{1-x}Cd_xTe$ materials, the existence of residual foreign-atom acceptor impurities and other crystalline defects is more prevalent than their short-wavelength counterparts due to their growth conditions, and one expects to find ample acceptor sites relevant to the present trap tunneling process throughout the bandgap irrespective of the p-type doping mechanism that is active in these materials. A Shockley-Read center located at ~30 meV above the valence band had been inferred earlier from temperature-dependent lifetime studies of highly compensated n-type $Hg_{1-x}Cd_xTe$ materials ($0.195 < x < 0.210$ and $N_D - N_A < 2 \times 10^{14}$ cm^{-3}) [19]. Recently, another such level located at ~10 meV above the valence band was identified from Hall measurement analysis of long-wavelength p-type $Hg_{1-x}Cd_xTe$ ($x < 0.2$) materials [17].

The present tunneling process for electrons from trap states on the p side to empty band states on the n side does not differ significantly from the conventional interband tunneling as far as the roles played by the potential barrier and the tunneling distance to the likelihood of the process occurring are concerned. The tunneling of an electron through a forbidden gap is formally the same as a particle tunneling through a potential barrier. The tunneling probability is relatively insensitive to the shape of the barrier; i.e., whether it is triangular, parabolic, or some other form. The important parameters are the effective mass of the tunneling electrons and the height and width of the barrier itself, which are determined by the doping concentrations of the junction and the junction impurity profile. The effective mass of electrons is smaller for long-wavelength $Hg_{1-x}Cd_xTe$ materials than for shorter wavelength materials. Consequently, the tunneling probability is greatly enhanced for photodiodes made out of the longer wavelength materials as will be discussed in Section III below. The trap sites on the p side from which the electrons tunnel to the band states on the n side are located physically very close to the junction depletion region so that the tunneling distance is about the same as that for direct interband tunneling.

As with direct band-to-band tunneling, the transverse momentum of the tunneling electrons must be included in the

calculation of the tunneling probability in order to conserve total momentum. For the present trap tunneling case, this can be viewed in much the same way as in conventional, direct interband tunneling whereby the total energy of the electron is divided into E_x and $E_\perp$ where $E_\perp$ is the energy associated with the momentum perpendicular to the direction of tunneling (or the transverse momentum), and E_x is the energy associated with momentum in the tunneling direction. The overall tunneling probability thus consists of two factors, namely, one which reflects the probability of tunneling with zero transverse momentum multiplied by another one which takes into consideration the effect of perpendicular energy. This formulation brings forth the importance of both the electron effective mass and the bandgap of the material on the tunneling probability. For long-wavelength $Hg_{1-x}Cd_xTe$ materials in which both the bandgap and electron effective mass are small, the tunneling probability can readily be seen to be appreciably large.

While the number of populated trap states on the p side of the junction is important for the present trap tunneling process, the availability of empty band states on the n side is equally significant for completing the process. The density of empty final states is strictly a function of the location of the quasi-Fermi level on the n side. This, in turn, depends upon the doping concentrations and the biasing condition of the device p-n junction. Fig. 2(a), (b), and (c) shows the p-n junction energy-band diagrams for $Hg_{0.8}Cd_{0.2}Te$ at three different p- and n-side doping concentrations. Also shown in these figures are three sets of hypothetical acceptor trap levels on the p side, labeled type ①, ②, and ③, respectively, in decreasing order of activation energy measured from the top of the valence band. As expected from the discussion presented earlier, type ③ traps being closer to the valence band edge than the other two types are more numerous than types ② and ①. Similarly, type ② traps are larger in number than type ①. The relative abundance of these three types of traps is also schematically represented in Fig. 2(a), (b), and (c). The λ_{co} for these photodiodes, as illustrated in these figures, at the temperature shown (40 K) is approximately 14 μm. For lightly doped p and n side as shown in Fig. 2(a) ($p \sim n \sim 5 \times 10^{14}$ cm^{-3}), empty band states are available at zero bias only to electrons occupying types ② and ① traps but not type ③ traps. However, when the junction is reverse biased by an amount qV, empty band states start to become available for type ③ traps, as depicted also in Fig. 2(a). For moderately doped p and n sides, as shown in Fig. 2(b) ($p \sim 5 \times 10^{15}$ cm^{-3} and $n \sim 1 \times 10^{16}$ cm^{-3}), the same situation prevails as in the lightly doped case except for the fact that a much smaller reverse bias would provide sufficient empty band states on the n side for the trap tunneling process to become significant. For heavily doped p and n sides ($p \sim 1 \times 10^{16}$ cm^{-3} and $n \sim 1 \times 10^{18}$ cm^{-3}) as shown in Fig. 2(c), one can see that empty band states on the n side are always available for the trap tunneling process to take place irrespective of any bias conditions prevalent at the device p-n junction.

From the discussion presented above it becomes apparent that electron tunneling via traps is not only a viable process in long-wavelength $Hg_{1-x}Cd_xTe$ photodiodes, but it can also

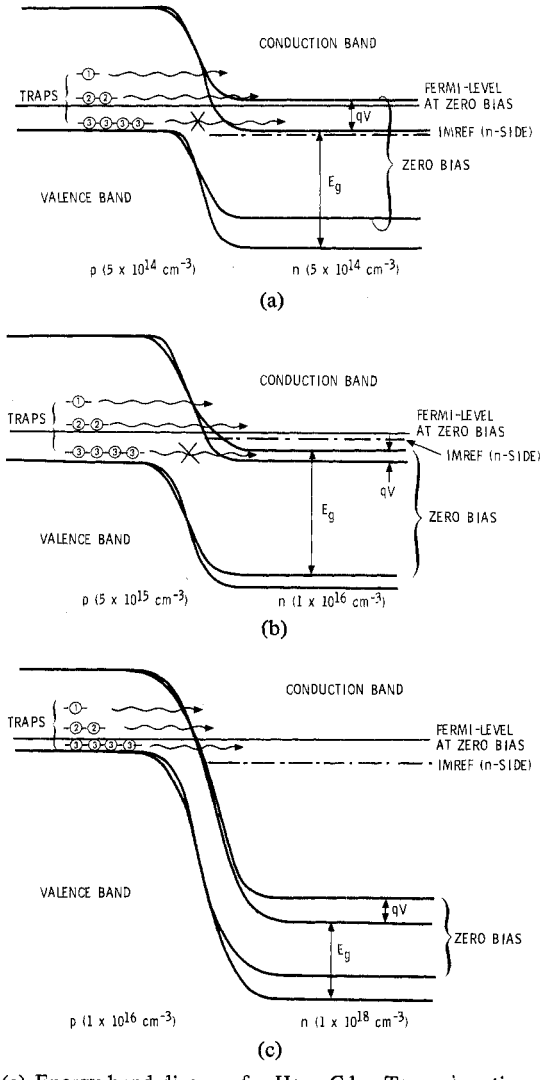

Fig. 2. (a) Energy band diagram for $Hg_{0.8}Cd_{0.2}Te$ p-n junction at 40 K with $N_A = 5 \times 10^{14}$ cm^{-3} and $N_D = 5 \times 10^{14}$ cm^{-3} (not drawn to scale). (b) Energy band diagram for $Hg_{0.8}Cd_{0.2}Te$ p-n junction at 40 K with $N_A = 5 \times 10^{15}$ cm^{-3} and $N_D = 1 \times 10^{16}$ cm^{-3} (not drawn to scale). (c) Energy band diagram for $Hg_{0.8}Cd_{0.2}Te$ p-n junction at 40 K with $N_A = 1 \times 10^{16}$ cm^{-3} and $N_D = 1 \times 10^{18}$ cm^{-3} (not drawn to scale).

be a significant current mechanism contributing to shot noise if the factors governing the probability of such a process are favorable. The effect of such a trap tunneling process on the performance of long-wavelength $Hg_{1-x}Cd_xTe$ photodiodes will be quantitatively explored in the next two sections.

III. A Parametric Trap Tunneling Model

We shall develop in this section a parametric trap tunneling model which can be used to calculate the tunneling current via traps in long-wavelength $Hg_{1-x}Cd_xTe$ photodiodes. The same model will be used to calculate the trap tunneling limited R_0A products for these devices under different material preparation and photodiode fabrication conditions. The actual computation of the R_0A products will be presented in the next section.

The energy-band diagram for a photodiode p-n junction illustrating the present trap tunneling model at zero bias and at a reverse bias of qV is shown schematically in Fig. 3. In this

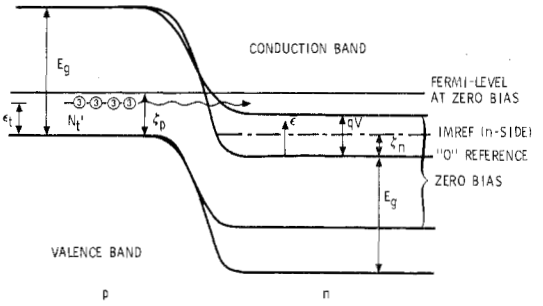

Fig. 3. Energy band diagram for HgCdTe p-n junction at arbitrary temperature T illustrating the mechanism of electron tunneling via acceptor traps.

figure, the carrier concentration on the p and n side of the junction is labeled p and n, respectively. E_g is the bandgap of the photodiode material at temperature T. The Fermi level at zero bias measured from the top of the valence band on the p side is designated ζ_p. ζ_n and ϵ are the quasi-Fermi level at a reverse bias of qV and the electron energy, respectively, measured from the valence band edge on the n side.

As discussed in Section II above, although the existence of acceptor traps in p-type $Hg_{1-x}Cd_xTe$ material can be safely assumed, the density of such traps and their energy distribution in the forbidden gap cannot readily be determined. Furthermore, the density and the energy distribution of these traps are likely to vary as a function of material composition x and might even take on different values for materials with the same composition but prepared at different times or with different techniques. In order to develop a trap tunneling model that is useful for quantitatively estimating the tunneling current, both of these quantities will be treated as parameters which can take on any hypothetically assumed values. The density of traps will be designated as N_t and the effective density of traps, namely, those traps that are filled with electrons N_t'. At the same time, it is assumed that all these acceptor traps are located at energy ϵ_t (see Fig. 3) above the top of the valence band on the p side. To complete the characterization of the present trap tunneling model one more parameter needs to be introduced. This parameter is the matrix element $W_t = (\phi_t \mid \nu_t \mid \psi_0)$ of the trap potential energy ν_t, in excess of the crystal potential taken between the unnormalized trap state wavefunction ϕ_t, and the conduction band-edge Bloch wavefunction ψ_0, normalized to unit volume. The significance of W_t and the role it plays in the trap tunneling process will become apparent as the model is further developed in the following paragraphs.

The development of the present trap tunneling model follows closely the formulation by Sah for treating the case of excess currents in gold-doped narrow silicon junctions [18]. Two major differences exist, however, between the present treatment and that by Sah for electron tunneling via traps. First, Sah's treatment emphasized electron tunneling via traps in the forward-bias region as an attempt to account for the large amounts of excess current observed in gold-doped silicon tunnel junctions. In the present treatment, we are interested only in the magnitude of the trap tunneling current that degrades the performance of photodiodes in the reverse-bias region. Second, the type of trap tunneling processes considered by Sah involves electrons tunneling between a trap state and a band state within the space charge of the junction. In other words, the active traps are physically located within the depletion region. For the present case, the majority of the acceptor traps participating in the trap tunneling process reside close to but not inside the space-charge region. Although the Sah-type acceptor traps that are located within the depletion region, and whose occupancy is, therefore, subjected only to Hall-Shockley-Read type process, do contribute to the present trap tunneling mechanism, their effect is expected to be small due to their relatively small number and the occupancy factor. These traps will not be included in our present model, but the effect of leaving them out in our subsequent R_0A product calculations will be assessed in Section V.

The transition probability rate w for an electron tunneling out of the trap to the conduction band is given by the well-known expression

$$w = \frac{2\pi}{\hbar} |M|^2 \rho(\epsilon) \tag{1}$$

where $\rho(\epsilon)$ is the density of final state in the conduction band and M is the matrix element linking the initial and final states for the perturbation causing the transition. Such an effective first-order matrix element for this electron tunneling process had been derived by Price [20] and is given by

$$M = W_t \left(\frac{v_x}{2V_c u_t}\right)^{1/2} e^{-\theta} \tag{2}$$

where W_t is the matrix element $(\phi_t \mid \nu_t \mid \psi_0)$ of the trap potential energy ν_t in excess of the crystal potential taken between the unnormalized trap-state wavefunction ϕ_t, and the conduction band-edge Bloch wavefunction ψ_0, normalized to unit volume; $\hbar u_x = |\partial E/\partial k_x|$, and u_t is evaluated at the trap; v_x is the component of the electron velocity at infinity in the conduction band; V_c is the volume of the crystal; and

$$\theta = \int |k_x| \, dx \tag{3}$$

where the integration covers the forbidden path.

Following the treatment by Sah [18] and assuming both an isotropic effective mass for electrons in $Hg_{1-x}Cd_xTe$ and a constant field approximation across the junction, (1) can be shown to be

$$w = \frac{\pi^2}{\hbar^3} \frac{m_e}{(E_g - \epsilon_t)} F_t W_t^2 \exp\left[-\frac{4}{3}\frac{(2m_e)^{1/2}}{\hbar F_t}(E_g - \epsilon_t)^{3/2}\right] \times \left\{1 - \exp\left[-\frac{2(2m_e)^{1/2}}{\hbar F_t}(E_g - \epsilon_t)^{1/2} \cdot \epsilon\right]\right\} \tag{4}$$

where m_e is the effective mass of the electron, ϵ_t is the location of the traps measured from the top of the valence band on the p side, W_t is the matrix element of the trap potential in excess of the crystalline component described before, F_t is the force on the electron at the trap site, and ϵ is the energy of the tunneled electron in the conduction band on the n side introduced earlier. The first exponential term in (4) can be identified as the tunneling probability, and the term involving the

second exponential reflects the effect of the density of final states in the transition probability.

Assuming the nonexistence of any processes that limit the filling rate for the acceptor traps on the p side, the trap tunneling current density may be obtained from

$$J_t = \int qN_t' w d\epsilon / F_t \tag{5}$$

where q is the electronic charge and N_t' is the effective density of traps. Substituting (4) for w into (5) and integrating over all possible electron energies in the final state we have

$$J_t = qN_t' \frac{\pi^2}{\hbar^3} m_e W_t^2 \exp\left[-\frac{4}{3}\frac{(2m_e)^{1/2}}{\hbar F_t}(E_g - \epsilon_t)^{3/2}\right] \times \int_0^{\zeta_p+\zeta_n-qV-\epsilon_t-E_g} \left[1 - \exp\left(-\frac{\epsilon}{E_\perp}\right)\right] d\epsilon \tag{6}$$

where

$$E_\perp \equiv \hbar F_t / \{[2m_e(E_g - \epsilon_t)]^{1/2}\} \tag{7}$$

ζ_p and ζ_n are the Imrefs on the p and n side of the junction, respectively, and V is the bias (negative for reverse), all defined earlier (see Fig. 3).

With the exception of N_t', ϵ_t, and W_t, which are introduced as parameters for the present trap tunneling model, all the other quantities appearing in (6) and (7) can be determined once the doping concentrations on both sides of the photodiode junction and the junction profile are specified. Equations (6) and (7) will be used together with the material and device parameters for calculating the trap tunneling limited R_0A products for long-wavelength $Hg_{1-x}Cd_xTe$ photodiodes in the next section.

IV. Trap Tunneling Limited R_0A Calculations

With the parametric trap tunneling model developed in Section III one can now calculate the trap tunneling limited R_0A products for long-wavelength $Hg_{1-x}Cd_xTe$ photodiodes with different p- and n-side doping concentrations and at different temperatures as a function of trap density, trap location, and junction impurity concentration gradient. However, to carry out such a calculation requires several additional computational steps. In the following paragraphs these steps are first outlined before the actual computations for the R_0A products.

The first step in the R_0A product calculation is to assign a value for the material composition x for $Hg_{1-x}Cd_xTe$. Since the compositional and temperature dependences for the bandgap E_g of $Hg_{1-x}Cd_xTe$, as determined by detector cutoff wavelengths, are known to a good degree of accuracy [21], the composition x determines the bandgap and hence the λ_{co} for photodiodes fabricated out of these materials. The present work will be concentrating on $Hg_{1-x}Cd_xTe$ materials with $x = 0.2$. This corresponds to a λ_{co} of $\sim$12 μm at 100 K.

The next step in the calculation is to set the values for the doping concentrations on both sides of the photodiode p-n junction, namely, N_A on the p side and N_D on the n side. For the n side, the donor levels are assumed to be shallow enough so that no freezeout of electrons occurs in the temperature range of interest (100 to 10 K). For the p side, the location of the acceptor levels is assumed to be at ϵ_t above the valence band edge and is treated as a parameter for the present trap tunneling model. The Fermi levels at zero bias on both the p and n side are then calculated using the well-known charge neutrality equation [22]. The nonparabolicity of the conduction band is taken into account by using the $k \cdot p$ method (Kane model) [23] to determine the electron concentration n. The interband matrix element for $Hg_{1-x}Cd_xTe$ used in the $k \cdot p$ calculation is taken to be 9×10^{-8} eV $\cdot$ cm. Statistics appropriate to impurity semiconductors are used for calculating the contribution by the acceptors to the hole concentration on the p side. The effective mass for holes is assumed to be independent of composition x and temperature, and is taken to be 0.55 m where m is the free electron mass [21]. This calculation for the Fermi levels has to be repeated for every temperature T, as E_g varies with the latter. The calculation of the Fermi levels also leads to the determination for the electron and hole concentrations on both sides of the p-n junction.

The next step in the sequence of calculational steps for the R_0A product is the determination of the electron effective mass for $Hg_{1-x}Cd_xTe$ ($x = 0.2$ in the present case) as a function of temperature. It is interesting to note that the Kane model used in the Fermi levels calculation described in the previous paragraph does not use an electron effective mass explicitly [23]. To preserve Kane's formalism for treating the nonparabolicity of the conduction band for $Hg_{1-x}Cd_xTe$, a parabolic equivalent electron effective mass was used in the calculation following the work of Schmit [21]. Although the use of this effective mass might not necessarily be valid for the present trap tunneling calculations, the uncertainty involved in its use as assessed by comparing its value with that of the parabolic effective mass is relatively small. The discussion of this is presented in Section V.

The final step in the sequence of calculations is to characterize the junction impurity profile for the $Hg_{1-x}Cd_xTe$ photodiodes. Two types of junction profiles will be considered, namely, the abrupt junction and a linearly graded junction characterized by the impurity concentration gradient a. The knowledge of the junction profile, together with the built-in potential obtained from the Fermi level calculations, the externally applied bias and the location of the acceptor traps, enables both the width of the junction and the force exerted on the electrons at the trap sites to be determined.

The calculational steps outlined above provide the means for computing all the quantities appearing in (6) and (7) for the trap tunneling current density J_t. R_0A product is then obtained by calculating J_t as a function of reverse bias in small incremental steps about the zero-bias origin. In this way, the trap tunneling limited R_0A products for long-wavelength $Hg_{1-x}Cd_xTe$ photodiodes were calculated with different p- and n-side doping concentrations and at different temperatures as a function of p-side trap density, trap location, and junction impurity concentration gradient. The results for these calculations are presented in the following.

Fig. 4 shows the trap tunneling limited R_0A products as a function of temperature for $Hg_{0.8}Cd_{0.2}Te$ photodiodes with

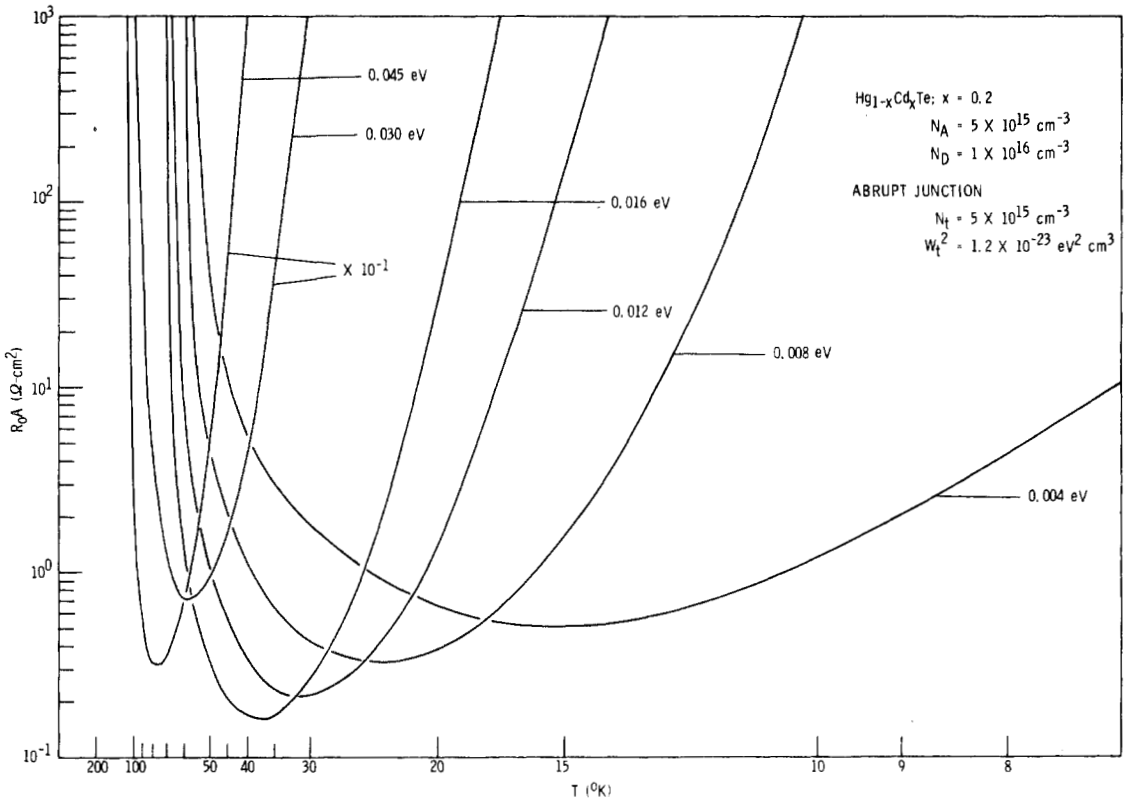

Fig. 4. Trap tunneling limited R_0A products versus temperature curves for $Hg_{0.8}Cd_{0.2}Te$ photodiodes with the location of acceptor traps ϵ_t as variable parameter.

the location of the acceptor traps ϵ_t above the top of the valence band on the p side as a variable parameter. The acceptor and donor concentration on the p and n side of the photodiode is 5×10^{15} cm^{-3} and 1×10^{16} cm^{-3}, respectively. The junction profile is assumed to be abrupt with an area equal to 1×10^{-4} cm^2. Although the trap density N_t is set equal to the acceptor concentration, the effective trap density N_t' is a function of the quasi-Fermi level ζ_p on the p side of the junction

$$N_t' = N_t \Big/ \left[1 + \frac{1}{2} \exp\left(\frac{-E_g + \epsilon_t - \zeta_p}{kT}\right)\right].$$

The matrix element W_t^2 is set equal to 1.2×10^{-23} eV$^2 \cdot$ cm^3 which is reasonable for acceptor-type traps in the Zinc Blende lattice as estimated experimentally by Sah and others [18], [24]. From Fig. 4 it can be seen that all the R_0A curves go through a characteristic minimum at some temperature T irrespective of the value assumed by ϵ_t. However, the temperature at which this minimum occurs shifts to a lower and lower temperature as ϵ_t assumes a smaller and smaller value. At the same time, the value for the R_0A product at the minimum increases as ϵ_t decreases. The occurrence of this minimum for the R_0A curves can be attributed to the gradual freezeout of the acceptor traps as the Fermi level shifts toward the top of the valance band on the p side at lower and lower temperatures. When this happens, the effective trap density N_t' decreases sharply leading to a vanishingly small trap tunneling current. On the other hand, at higher temperatures, the values for both the electron effective mass m_e and the bandgap E_g increase leading to a much smaller tunneling probability and overlap integral with a concomitant decrease in the tunneling current and a rapidly increasing R_0A.

The effect of the p- and n-side doping concentrations on the trap tunneling limited R_0A products as a function of temperature for $Hg_{0.8}Cd_{0.2}Te$ photodiodes with abrupt junctions is shown in Fig. 5. Three sets of R_0A curves are shown corresponding to N_A equal to 1×10^{16} cm^{-3}, 5×10^{15} cm^{-3}, and 5×10^{14} cm^{-3} and N_D equal to 1×10^{18} cm^{-3}, 1×10^{16} cm^{-3}, and 5×10^{14} cm^{-3}, respectively. The junction area for these diodes is again 1×10^{-4} cm^2 and the value for W_t^2 is the same as in Fig. 4. Three different values for the trap location are included in each set of the R_0A curves corresponding to 0.004, 0.016, and 0.045 eV above the top of the valence band, respectively. It can be seen from Fig. 5 that the effect of lower doping concentrations on both sides of the junction tends to shift the R_0A minima to lower temperatures but significantly increase the R_0A values at the minima.

Fig. 6 shows the trap tunneling limited R_0A curves as a function of temperature for $Hg_{0.8}Cd_{0.2}Te$ photodiodes with both abrupt and linearly graded junction profiles. The doping concentration on the p and n side is 1×10^{16} cm^{-3} and 1×10^{18} cm^{-3}, respectively, with the location of the traps set at 0.016 eV above the valence band edge. The device junction area and the value for W_t^2 are the same as those for Figs. 4 and

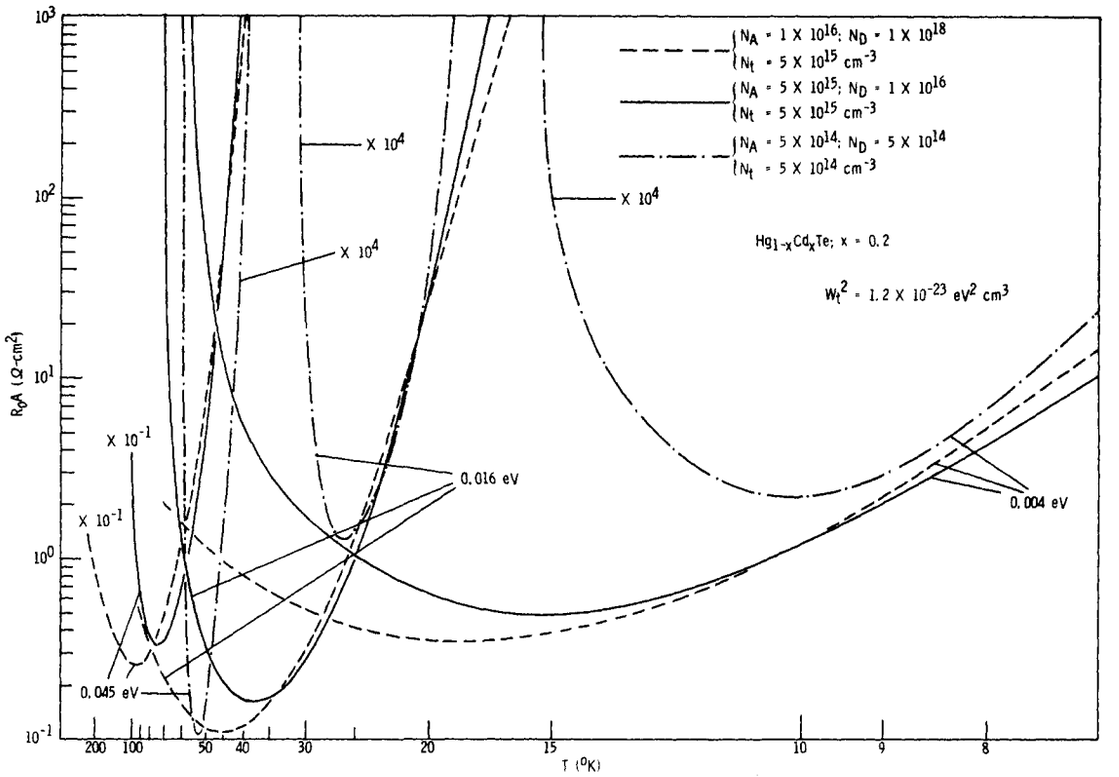

Fig. 5. Trap tunneling limited R_0A products versus temperature curves for $Hg_{0.8}Cd_{0.2}Te$ photodiodes, showing the effect of doping concentrations on both sides of the p-n junction.

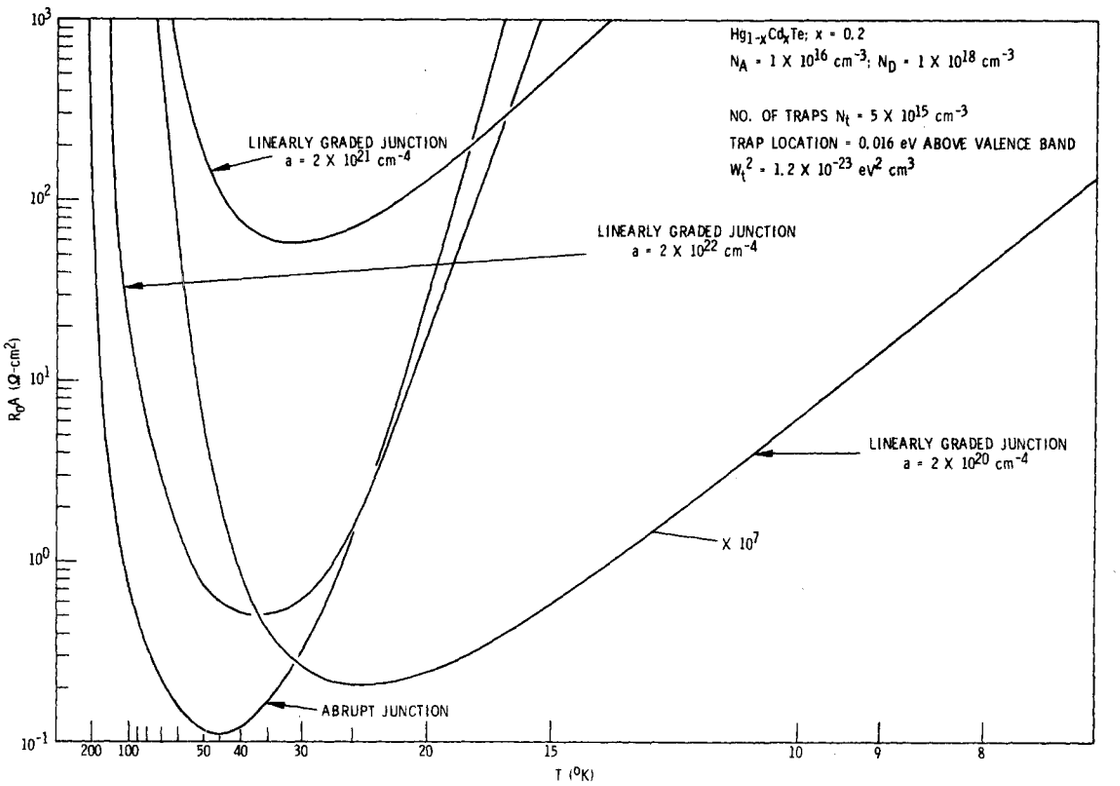

Fig. 6. Trap tunneling limited R_0A products versus temperature curves for $Hg_{0.8}Cd_{0.2}Te$ photodiodes showing the effect of p-n junction impurity profile.

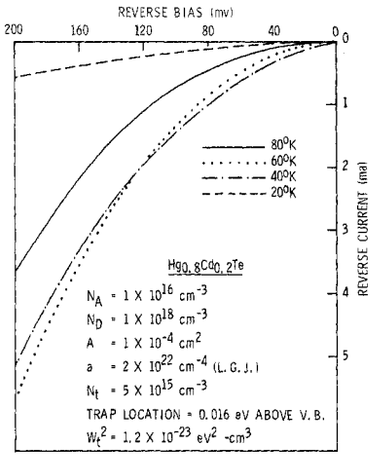

Fig. 7. Trap tunneling limited reverse I-V characteristics at different temperatures for a $Hg_{0.8}Cd_{0.2}Te$ photodiode with $N_A = 1 \times 10^{16}$ cm^{-3} and $N_D = 1 \times 10^{18}$ cm^{-3} (see text for other parameter values).

5. It can be seen from Fig. 6 that the effect of a more gradual junction profile as reflected by a smaller junction impurity concentration gradient a is again to shift the minimum of the R_0A curve to a lower temperature, and significantly increase the R_0A value for the minimum.

Fig. 7 shows the calculated trap tunneling limited reverse I-V characteristics for a $Hg_{0.8}Cd_{0.2}Te$ photodiode at temperatures of 80, 60, 40, and 20 K, respectively. The parameters used are exactly the same as those used in Fig. 6 with the exception of the junction impurity concentration gradient a which is taken to be 2×10^{22} cm^{-4}. In addition to the soft reverse-breakdown characteristics for these I-V curves, the reverse saturation current first increases as a function of decreasing temperature but then decreases again at around 40 K. This peculiar temperature behavior of the reverse saturation current can be directly linked to the occurrence of the minimum in the trap tunneling limited R_0A versus temperature plots presented earlier in Fig. 4.

V. Discussion

Presented in this paper is the development of a parametric trap tunneling model based on the formulation by Sah for investigating the effect of electron tunneling via traps on the detector performance of long-wavelength $Hg_{1-x}Cd_xTe$ photodiodes. Specifically, the trap tunneling limited R_0A products as a function of temperature were calculated for $Hg_{0.8}Cd_{0.2}Te$ with different p- and n-side doping concentrations, junction profiles, and locations of acceptor trap levels on the p side. The calculated R_0A versus temperature curves as presented in Section IV all exhibit a characteristic minimum in R_0A value at a temperature somewhere between 80 and 15 K dependent on the trap location. This is in good agreement with the temperature dependence of measured R_0A products at low temperatures for typical long-wavelength $Hg_{1-x}Cd_xTe$ photodiodes such as those shown in Fig. 1. In comparing the theoretical curves of Figs. 4–6 with experimental data such as those shown in Fig. 1, it must be remembered that the R_0A values obtained from the trap tunneling calculations depend strongly on such parameters as the trap density N_t, the location of the trap levels ϵ_t, and the matrix element W_t^2. Although the theoretical results can be fitted precisely to the experimental data by appropriately adjusting the parameters mentioned above, such an exercise is rather meaningless, at least to the extent that the calculated R_0A curves can be translated up and down at will in such a maneuver. The crucial evidence in support of the presently proposed trap tunneling mechanism lies rather in its correct prediction of the somewhat unexpected temperature dependence of the measured R_0A products at low temperatures. Such a trap tunneling mechanism also predicts a soft reverse-breakdown characteristic for these photodiodes and a reverse saturation current which goes through a maximum at about the same temperature as that for the minimum of the R_0A curve. Experimentally, these latter predictions had also been observed to be true for typical long-wavelength $Hg_{1-x}Cd_xTe$ photodiodes [15].

During the course of our model development, a number of assumptions had been made which require further discussion. As mentioned in Section III, the present model precludes the contribution to the trap tunneling current by acceptor traps that reside physically within the junction space-charge region. A rough order-of-magnitude calculation indicates that the contribution by these additional traps to the overall tunneling current is relatively small. This conclusion is based on an estimate of the density of these traps and their filling factor which is governed solely by the Hall-Shockley-Read type recombination statistics. The present model also ignores the effect of band-edge tails in the trap tunneling process. This is justified in view of the fact that the photodiodes considered here are not tunnel diodes, and the p- and n-side doping concentrations are not large enough for these band-edge tails to modify the overall band structure to an appreciable degree.

When considering the acceptor traps on the p side, the current model assumes that all these traps are located at only one energy level, namely, ϵ_t above the valence band edge. Such an assumption is clearly not justified. However, the inclusion of an energy distribution for these traps or even the possibility that more than one set of traps located at various levels participate in the tunneling process only serves to add to the complexity of the current calculations without providing any new physical insights to the problem. Nevertheless, such possibilities should not be left out in future more refined model developments. Much of the same argument applies also to the adoption of a parabolic equivalent electron effective mass in the Fermi levels calculation for $Hg_{1-x}Cd_xTe$. Although the electron effective mass for $Hg_{1-x}Cd_xTe$ can safely be taken as isotropic since the conduction-band minimum occurs at the center of the Brillouin zone its dependence upon temperature and composition x has yet to be investigated, both theoretically and experimentally, in greater detail. A better known electron effective mass for $Hg_{1-x}Cd_xTe$ materials will no doubt lead to further refinement of the present trap tunneling model.

While the present calculation clearly points to the fact that electron tunneling via traps can in some cases limit the ultimate detector performance for long-wavelength $Hg_{1-x}Cd_xTe$ photo-

diodes at low temperatures in much the same manner as diffusion and g-r mechanisms do at higher temperatures, it also provides some useful device design guidelines for minimizing such impacts. The calculated results summarized in Figs. 4-6 suggest that both lower doping concentrations and a more gradual junction impurity profile will lead to smaller trap tunneling currents and, consequently, higher attainable R_0A products. Such prescriptions, however, at present might be still a bit premature as the sources for all the other leakage current mechanisms (both surface and bulk) that are active in long-wavelength $Hg_{1-x}Cd_xTe$ photodiodes remain mostly unidentified.

The electron trap tunneling mechanism considered presently is by and large a bulk process. This process, however, is anticipated to become more dominant near the device surface due to the expected increase in defect density, especially for materials like $Hg_{1-x}Cd_xTe$. One of the current impeti in long-wavelength $Hg_{1-x}Cd_xTe$ photodiode detector research and development is for improved R_0A products by the elimination of device leakage currents. The major difficulty confronting this effort is the identification of the sources for these observed leakage currents. The separation of the surface from the bulk leakage is one of the first tasks that has to be addressed. The current development for the trap tunneling model is but a small step in this direction. Despite the apparent success in its ability to account for certain features in the measured R_0A data as a function of temperature as mentioned earlier the present model requires further development, both in theoretical treatment and in more concrete verifications. More direct comparisons between calculated results and measured data obtained from devices fabricated with carefully controlled parameters, such as doping concentrations and junction profile, are needed for further testing the present model. In addition, separate experiments such as deep level transient spectroscopy (DLTS), photoluminescence, carrier lifetime studies, etc., are required to pin down the exact location of the acceptor traps in the forbidden gap of p-type $Hg_{1-x}Cd_xTe$ materials. Until such time that the present model can be unequivocally established, it will remain difficult to separate surface from bulk leakage current mechanisms and also to further improve the performance of these devices.

Acknowledgment

The author wishes to thank those members of the Santa Barbara Research Center staff who encouraged and advised him. Special thanks go to P. R. Bratt who first suggested the current problem and subsequently aided the author in many ways for preparing this manuscript. Thanks are also due to A. H. Lockwood, K. J. Riley, and J. D. Langan for many helpful discussions.

References

[1] A. F. Milton and M. Hess, "Series-parallel scan IR CID focal plane array concept," in *CCD-75 Proc.*, (San Diego, CA, Oct. 1975), pp. 71–83.
[2] D. F. Barbe, "Advanced infrared focal plane array concepts," *Electro-Op. Sys. Des.*, pp. 50–58, Apr. 1977.
[3] J. T. Longo, D. T. Cheung, A. M. Andrews, C. C. Wang, and J. M. Tracy, "Infrared focal planes in intrinsic semiconductors," *IEEE Trans. Electron Devices*, vol. ED-25, pp. 213–232, Feb. 1978.
[4] J. C. Kim, "InSb charge-injection device imaging array," *IEEE Trans. Electron Devices*, vol. ED-25, pp. 232–241, Feb. 1978.
[5] A. M. Andrews, "Hybrid infrared imaging arrays," in *IEDM Tech. Dig.*, pp. 505–508, Dec. 1978.
[6] R. M. Hoendervoogt, K. A. Kormos, J. P. Rosbeck, J. R. Toman, and C. B. Burgett, "Hybrid InSb focal plane array fabrication," in *IEDM Tech. Dig.*, pp. 510–512, Dec. 1978.
[7] W. J. Parrish, F. J. Renda, N. L. Ray, D. G. Maeding, R. E. Eck, and J. R. Toman, "Characterization of a 32 × 32 InSb hybrid IR focal plane," in *IEDM Tech. Dig.*, pp. 513–516, Dec. 1978.
[8] J. P. Rode, J. D. Blackwell, A. M. Andrews, R. J. Eisel, G. M. Williams, and W. E. Tennant, "InAsSb hybrid focal plane for infrared images," in *Proc. IRIS, Detector Specialty* (Annapolis, MD, June 1978).
[9] K. Nummedal, J. C. Fraser, S. C. Su, R. Baron, and R. M. Finnila, "Extrinsic silicon monolithic focal plane array technology and applications," in *CCD '75 Proc.* (San Diego, CA, Oct. 1975), pp. 19–30.
[10] R. D. Thom, F. J. Renda, W. J. Parrish, and T. L. Koch, "Monolithic InSb charge-coupled infrared device," in *IEDM Tech. Dig.*, pp. 501–504, Dec. 1978.
[11] D. D. Buss, R. A. Chapman, M. A. Kinch, S. R. Borello, A. Simmons, and C. G. Roberts, "Infrared monolithic HgCdTe IR CCD focal plane technology," in *IEDM Tech. Dig.*, pp. 496–500, Dec. 1978.
[12] M. B. Reine and R. M. Broudy, "Review of HgCdTe infrared detector technology," *Proc. Soc. Photo-Op. Instr. Eng.*, vol. 124, pp. 91–101, Aug. 1977.
[13] K. J. Riley, A. H. Lockwood, and P. R. Bratt, "Photovoltaic HgCdTe research and development at SBRC," in *Proc. IRIS, Detector Specialty* (Annapolis, MD, June 1978).
[14] K. J. Riley, P. R. Bratt, and A. H. Lockwood, "Large area PV HgCdTe quadrant arrays for laser detection at 10.6 μm," in *Proc. IRIS, Detector Specialty* (Annapolis, MD, June 1978).
[15] R. J. Briggs and M. B. Reine, "Feasibility of photovoltaic HgCdTe for very long wavelength applications," Interim Tech. Rep., AFML Contract F33615-77-C-5197, Sept. 1978.
[16] J. Y. Wong and E. E. Loebner, "Tunneling contribution to noise in small bandgap photovoltaic detectors," *Bull. APS II*, vol. 17, p. 61, 1972.
[17] K. J. Riley and P. R. Bratt, private communication.
[18] C. T. Sah, *Phys. Rev.*, vol. 123, p. 1594, 1961.
[19] M. A. Kinch, M. J. Blau, and A. Simmons, *J. Appl. Phys.*, vol. 44, p. 1649, 1973.
[20] P. J. Price, *Bull. Am. Phys. Soc.*, vol. 5, p. 160, 1960.
[21] J. L. Schmit, *J. Appl. Phys.*, vol. 41, p. 2876, 1970.
[22] J. S. Blakemore, *Semiconductor Statistics*. New York: Pergamon, 1960.
[23] E. O. Kane, *J. Phys. Chem. Solids*, vol. 1, p. 249, 1957.
[24] H. Brooks, *Advances in Electronics and Electron Physics*, L. Marton, Ed. New York: Academic Press, 1955.